Autonomous Hovering of an Experimental Unmanned Helicopter System with Proportional-Integral Sliding Mode Control

Chien-Hong Lin[1]; Shau-Shiun Jan[2]; and Fei-Bin Hsiao[3]

Abstract: This paper presents a method of approaching the attitude control of an autonomously hovering unmanned helicopter system. The proportional-integral sliding mode controller (PISMC) features a combination of the conventional sliding mode control (SMC) and the integral sliding mode control (ISMC). By applying the PISMC algorithm, the controller is capable of providing stable roll and pitch control of the main rotor simultaneously. To show how PISMC may improve system performance, this paper develops an experimental unmanned helicopter system to assess the performance of the proposed controller. The results of the simulation show that the tracking error of the PISMC is not only smaller but also converges more quickly than that of the conventional SMC. Resulting roll and pitch controllers are successfully verified in computer simulations and actual flight tests. The flight test results presented in the paper are found to be consistent with the simulation results. **DOI: 10.1061/(ASCE)AS.1943-5525.0000068.** *© 2011 American Society of Civil Engineers.*

CE Database subject headings: Sliding; Aircraft; Experimentation.

Author keywords: Sliding mode control; Autonomous hovering; Unmanned helicopter.

Introduction

Sliding mode control (SMC) has been widely accepted as an efficient method for tracking or performing attitude control of uncertain nonlinear systems. It has been shown in principle to achieve perfect performancein the presence of parameter uncertainties and bounded external disturbances.

The main structure of variable structure control (VSC) theory was proposed by a former USSR scholar (Utkin 1977). Owing to imperfect switching in practice, the chattering problem associated with the high-frequency oscillation of the system became unavoidable. To solve the problem, Slotine (1984) came up with the idea of suppressing chattering by guiding the systems' tracking into the boundary layer within a finite time. Also, an integral variable structure controller (IVSC) which is based on the first-order dynamic formula, was mentioned by Chern and Wu (1991). The feature of IVSC is the addition of an integrator into the sliding surface to manage the approaching mode of the electrohydraulic position servo control and to neutralize the inaccuracy of output in a steady system. The effect of IVSC is to decrease overshoot in the performance of a controller. However, the response of the controller is decelerated. Chen and Her (1992) introduced the bang-bang sliding mode (BBSM) control, which was a new sliding surface. They assumed that the initial situation is on the sliding surface. According to VSC theory, the system situation would not leave the converting surface as long as the trace was on the converting surface and approaching to the balance point along this surface. This might not be applicable to realistic control problems because initial situation cannot be obtained precisely in practical physical systems. Sira-Ramirez et al. (1994) proposed a dynamic, multivariable, discontinuous feedback control strategy of the sliding-mode type for the altitude stabilization of a nonlinear helicopter model in vertical flight. Utkin and Jingxin (1996) proposed a new sliding mode design concept named integral sliding mode control (ISMC). The difference between ISMC and conventional sliding mode design approaches is the integral form of the error term in place of the original error term. Fung et al. (1997) discussed a VSC that is able to switch between conventional and integral methods. This proposal shows a great improvement in control performance but is unstable because a considerable impulsive current might interfere with the system when switching. Yang and Kung (2000) developed a nonlinear H_∞ control system for helicopters to improve their flight performance and stability under a large flight envelope. Baik et al. (2000) designed an ISMC with one separate boundary surface to decrease chattering and improve the controllers' responses. Hess and Wells (2002) proposed a new SMC, which was a PID-type sliding surface for flight control design. Su and Wang (2002) designed a complementary SMC with two separate boundary surfaces to decrease chattering and improve the controllers' responses. In 2004, Sam et al. applied the design of proportional-integral SMC to active suspension system. Niu et al. (2005) applied the design of robust integral sliding mode control to uncertain stochastic systems. Waslander et al. (2005) applied the design of ISMC to multi-agent quad-rotor test beds. Moreover, Bouabdallah et al. (2005) applied back-stepping and sliding-mode techniques to indoor microquad rotors. Chen et al. (2008) proposed an adaptive sliding mode control (ASMC) of the synchronous reluctance motor (SynRM) position drive system to avoid high chattering. This method employed a Lyapunov function candidate to guarantee convergence and track the position command of the

[1]Ph.D. Student, Institute of Aeronautics and Astronautics, National Cheng Kung Univ., Taiwan.

[2]Professor, Institute of Aeronautics and Astronautics, National Cheng Kung Univ., Taiwan (corresponding author). E-mail: ssjan@mail.ncku.edu.tw

[3]Professor, Institute of Aeronautics and Astronautics, National Cheng Kung Univ., Taiwan.

Note. This manuscript was submitted on August 25, 2009; approved on June 30, 2010; published online on July 2, 2010. Discussion period open until December 1, 2011; separate discussions must be submitted for individual papers. This paper is part of the ***Journal of Aerospace Engineering***, Vol. 24, No. 3, July 1, 2011. ©ASCE, ISSN 0893-1321/2011/3-338–348/$25.00.

SynRM system asymptotically. Hu et al. (2009) applied the design of back-stepping SMC to dual-stage control systems.

This paper focuses on attitude PISMC for a small-scale unmanned helicopter. Although the concept of PISMC is similar to the models proposed by Utkin and Shi (1996), Su and Wang (2002), and Baik et al. (2000), it has a totally different application target and gives two complementary parameters for tuning the controller. The PISMC proposed in this study is suitable for an unmanned helicopter system. The main features of PISMC are that it combines SMC and ISMC and that it has superior tracking performance. In addition, this paper uses a nonlinear system as an example for demonstrating the method's tracking accuracy and mitigation of the chattering phenomenon. The design of PISMC is further applied to an unmanned helicopter system.

The flight dynamics of a helicopter are dominated by the main rotor and the tail rotor. For a radio-controlled (RC) helicopter, the collective and cyclic pitch angles of main blades are controlled by mechanical linkages, which are actuated by servos. The pitch angles' variation of the main blades produce complex aerodynamic loads and induce different orientation of the tip-path plane (TPP) formed by the rotating main rotor. By changing the magnitude and direction of the main rotor's thrust and the tail rotor's thrust, the helicopter can perform various flight maneuvers. In other words, the attitudes, especially the rolling and pitching, of the helicopter, are affected mainly by the main rotor's TPP orientation. However, the tail rotor is responsible for the heading of the helicopter.

In the following sections, we will introduce some characteristics of the SMC method and their drawbacks. On the basis of these understandings, the PISMC method is proposed. Before PISMC is applied to the real system, a nonlinear equation is used for simulations to demonstrate that the performance of PISMC is superior to that of SMC. This paper then derives the dynamic model of an experimental unmanned helicopter with given parameters. The PISMC is designed based on the helicopter's model, and all the input data is obtained from real flight tests. With the flight data, the PISMC generates corresponding control output, which is analyzed. Relevant results are discussed.

Proportional-Integral Sliding Mode Control

Conventional SMC is considered a proportional-type SMC. The control method works by guiding the state trajectory of the system state to slide into the predetermined sliding surface and finally reach the origin of the phase plane (Slotine 1991; Edwards 1998). When the state trajectory is sliding on the sliding surface, the corresponding dynamic performance of the system is governed by the equations of the sliding surface. There are two fundamental requirements for the SMC. The first is to design a sliding surface and to force the state trajectory to slide along that surface by using a switching control law. The second is to ensure that each of the tracking points on the sliding surface satisfies the sliding conditions. The switch of the control law is determined by the predefined switching conditions. With the help of the switching of the control signal, the trajectory can be guided into the region between the boundary layers and satisfy the sliding condition. After that, the state trajectory can move toward to the target point.

Consider a dynamic system described by a nth-order nonlinear differential equation:

$$\tilde{x}^{(n)} = f(\tilde{X}) + \tilde{u} \tag{1}$$

Assumption

Assume that f is not known exactly but can be written as

$$f = \hat{f} + \Delta f \tag{2}$$

where $\hat{f}$ = nominal part and Δf = uncertain part that is bounded by a known function $\tilde{f}$, i.e.,

$$|\Delta f| \le \tilde{F}(\tilde{X}, t), \qquad \forall \tilde{X}, t \tag{3}$$

The objective of the PISMC is to make the system's output

$$\tilde{X} = \begin{bmatrix} \tilde{x} & \dot{\tilde{x}} & \dots & \tilde{x}^{(n-1)} \end{bmatrix}$$

approaching a desired signal

$$\tilde{X}_d = \begin{bmatrix} \tilde{x}_d & \dot{\tilde{x}}_d & \dots & \tilde{x}_d^{(n-1)} \end{bmatrix}$$

The tracking error is defined as

$$E = \tilde{X} - \tilde{X}_d = \begin{bmatrix} e & \dot{e} & \dots & e^{(n-1)} \end{bmatrix}^T \tag{4}$$

When applying the PISMC, a sliding surface must be designed previously. Then the system trajectory can be guided toward the target point after entering the sliding surface. Based on the magnitude of errors, we can define a time-varying surface in state space belonging to R^n by the sliding surface $s_{PI}(\tilde{X}, t) = 0$. The sliding surface of the PISMC consists of two sliding surfaces: s_P is the proportional sliding surface, and s_I is the integral sliding surface. They are presented in the following forms:

$$s_P = \left(\frac{d}{dt} + \lambda\right)^{n-1} e, \qquad s_I = \left(\frac{d}{dt} + \alpha\right)^{n} \xi_e \tag{5}$$

where λ and α = complementary parameters and give two complementary parameters for tuning the gains of controller, $\lambda > 0$, $\alpha > 0$, $\xi_e(t) = \int_0^t e(\tau) d\tau$, and $s_{PI} = s_P + s_I$.

The equation $s_{PI}(\tilde{X}, t) = 0$ means a sliding surface passing through the origin of the phase plane. According to this equation, $s_{PI} = 0$ is a $(n-1)$th-order linear differential equation, and all the eigenvalues of the eigen equations are located in the left complex plane. Once the sliding surface has been determined, we can start to design the controller and define the sliding conditions as follows:

$$s_{PI} \dot{s}_{PI} \le -\eta |s_{PI}| \tag{6}$$

where $\eta > 0$ and $\dot{s}_{PI}$ denotes the derivative of s_{PI}.

The PISMC is designed as

$$\tilde{u} = \hat{u} + v_s \tag{7}$$

where

$$\hat{u} = -\hat{f} + \tilde{x}_d^{(n)} - \left[\sum_{m=0}^{n-2} \binom{n-1}{m} e^{(m+1)} \lambda^{(n-m-1)}\right] - \left[\sum_{m=0}^{n-1} \binom{n-1}{m} e^{(m+1)} \alpha^{(n-m-1)}\right] - \alpha \left[\sum_{m=0}^{n-1} \binom{n-1}{m} e^{(m)} \alpha^{(n-m-1)}\right] \tag{8}$$

$$v_s = -k \operatorname{sgn}(s_{PI}) \tag{9}$$

with

$$\mathrm{sgn}(s_{PI}) = \begin{cases} 1 & \text{if } s_{PI} > 0 \\ 0 & \text{if } s_{PI} = 0 \\ -1 & \text{if } s_{PI} < 0 \end{cases} \tag{10}$$

We summarize the controller design in the following theorem.

Theorem

If there is a k such that

$$k = \widetilde{F}(\widetilde{X}, t) + \eta \tag{11}$$

then there exists a $k > 0$ such that the PISMC [Eqs. (7)–(10)] stabilizes the system [Eq. (1)], and the tracking error as defined in Eq. (4) will tend to a neighborhood of zero within a finite time.

Proof

To prove that $\widetilde{u}$ satisfies the sliding conditions, the following Lyapunov function is employed:

$$\begin{aligned} V &= \frac{1}{2}s_{PI}^2 = \frac{1}{2}(s_P + s_I)^2 = \frac{1}{2}\left[\left(\frac{d}{dt}+\lambda\right)^{n-1} e + \left(\frac{d}{dt}+\alpha\right)^{n}\xi_e\right]^2 \\ &= \frac{1}{2}\left[\left(\frac{d}{dt}+\lambda\right)^{n-1} e + \left(\frac{d}{dt}+\alpha\right)^{n-1}\left(\frac{d}{dt}+\alpha\right)\xi_e\right]^2 \\ &= \frac{1}{2}\left[\left(\frac{d}{dt}+\lambda\right)^{n-1} e + \left(\frac{d}{dt}+\alpha\right)^{n-1}(e+\alpha\xi_e)\right]^2 \end{aligned} \tag{12}$$

We choose an appropriate $\widetilde{u}$ to satisfy $\dot{V} < 0$.

$$\begin{aligned} \dot{V} = s_{PI}\dot{s}_{PI} &= (s_P + s_I)(\dot{s}_P + \dot{s}_I) = \left[\sum_{m=0}^{n-1}\binom{n-1}{m} e^{(m+1)}\lambda^{(n-m-1)} + \sum_{m=0}^{n-1}\binom{n-1}{m} e^{(m+1)}\alpha^{(n-m-1)} + \alpha\sum_{m=0}^{n-1}\binom{n-1}{m} e^{(m)}\alpha^{(n-m-1)}\right](s_P + s_I) \\ &= \left[e^{(n)} + \sum_{m=0}^{n-2}\binom{n-1}{m} e^{(m+1)}\lambda^{(n-m-1)} + \sum_{m=0}^{n-1}\binom{n-1}{m} e^{(m+1)}\alpha^{(n-m-1)} + \alpha\sum_{m=0}^{n-1}\binom{n-1}{m} e^{(m)}\alpha^{(n-m-1)}\right](s_P + s_I) \\ &= \left[\widetilde{x}^{(n)} - \widetilde{x}_d^{(n)} + \sum_{m=0}^{n-2}\binom{n-1}{m} e^{(m+1)}\lambda^{(n-m-1)} + \sum_{m=0}^{n-1}\binom{n-1}{m} e^{(m+1)}\alpha^{(n-m-1)} + \alpha\sum_{m=0}^{n-1}\binom{n-1}{m} e^{(m)}\alpha^{(n-m-1)}\right](s_P + s_I) \\ &= \left[\hat{f} + \Delta f + \widetilde{u} - \widetilde{x}_d^{(n)} + \sum_{m=0}^{n-2}\binom{n-1}{m} e^{(m+1)}\lambda^{(n-m-1)} + \sum_{m=0}^{n-1}\binom{n-1}{m} e^{(m+1)}\alpha^{(n-m-1)} + \alpha\sum_{m=0}^{n-1}\binom{n-1}{m} e^{(m)}\alpha^{(n-m-1)}\right](s_{PI}) \\ &= [\Delta f - k\mathrm{sgn}(s_{PI})]s_{PI} \le |\Delta f||s_{PI}| - k|s_{PI}| \le -(k - \widetilde{F})|s_{PI}| \Rightarrow \dot{V} \le -(k - \widetilde{F})|s_{PI}| \end{aligned}$$

The condition $\dot{V} \le -\eta|s_{PI}|$ is demanded to ensure the stability of the system and satisfy the sliding conditions as in Eq. (6). This ensures that any trajectory $e(t)$ will converge to the neighborhood around origin of the phase plane, which stands for zero steady-state error.

In fact, there is a discontinuous switching function (sgn) of the discontinuous controller $v_s$in the control signal; this function is established by an infinitely large switching frequency. However, this infinitely large switching frequency cannot be realized in a real physical system. In this way, the state trajectory would oscillate around the two sides of $s_{PI} = 0$,which results in the chattering phenomenon.

To reduce the chattering problem, the concept of boundary range B is introduced as

$$B = \{\widetilde{X} | s_{PI}(\widetilde{X}, t) = \pm\Phi\}, \quad \Phi > 0 \tag{13}$$

The error phase plane of the boundary layer of the sliding surface, s_{PI}, coincides with the boundary range of ε. Note that Φ is the boundary layer and ε is the error of boundary range. Because the switch action cannot be completed instantaneously and the effect of delay exists, the state trajectory $\widetilde{X}$ would oscillate between the boundary layers. Fig. 1 shows the second-order error phase plane; the most common way of mitigating the oscillation is to replace the sliding surface with the boundary layers.

The switching law of controller v_s is designed as

$$v_s = -k\mathrm{sat}\left(\frac{s_{PI}}{\Phi}\right) \tag{14}$$

The function $\mathrm{sat}(s_{PI}, \Phi)$ is the saturation function defined by

$$\mathrm{sat}(s_{PI}, \Phi) = \begin{cases} s_{PI}/\Phi & \text{if } |s_{PI}| \le \Phi \\ \mathrm{sgn}(s_{PI}) & \text{if } |s_{PI}| > \Phi \end{cases} \tag{15}$$

Numerical Simulation Result

The numerical application of the proposed control schemes to the control of a simple example is presented using the MATLAB/SIMULINK software. To demonstrate the performance of the PISMC and to compare it with other methods, we consider a simple example from Slotine (1991), given as follows

$$\dddot{\widetilde{x}} + a(t)\dot{\widetilde{x}}^2\cos 3\widetilde{x} = \widetilde{u} \tag{16}$$

where the function $a(t)$ is unknown but verifies $1 \le a(t) \le 2$. One has $\hat{f} = -1.5\dot{\widetilde{x}}^2\cos 3\widetilde{x}$ and $\widetilde{F} = 0.5\dot{\widetilde{x}}^2|\cos 3\widetilde{x}|$.

We compare the performance of control in a simple example with two types of sliding mode control methods. These methods are (1) SMC and (2) PISMC.

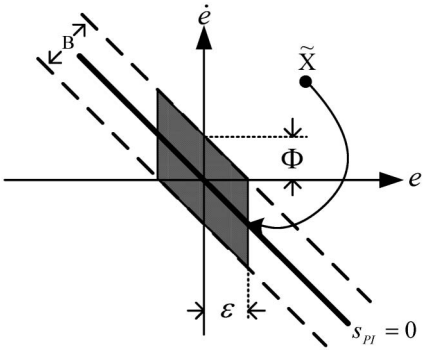

Fig. 1. Illustration of the boundary layer for a sliding surface

(1) Conventional SMC method

$$\widetilde{u} = 1.5\dot{\widetilde{x}}^2 \cos 3\widetilde{x} + \ddot{\widetilde{x}}_d - \lambda e - \lambda\dot{e} - \ddot{e} - \left(0.5\dot{\widetilde{x}}^2|\cos 3\widetilde{x}| + \eta\right)\text{sat}\left(\frac{s}{\Phi}\right)$$

where

$$s = \dot{e} + \lambda e$$

(2) PISMC method

$$\widetilde{u} = 1.5\dot{\widetilde{x}}^2 \cos 3\widetilde{x} + \ddot{\widetilde{x}}_d - \alpha^2 e - (\lambda + 2\alpha)\dot{e} - \ddot{e} - \left(0.5\dot{\widetilde{x}}^2|\cos 3\widetilde{x}| + \eta\right)\text{sat}\left(\frac{s_P + s_I}{\Phi}\right)$$

where

$$s_P = \left(\frac{d}{dt} + \lambda\right) e = \dot{e} + \lambda e$$

$$s_I = \left(\frac{d}{dt} + \alpha\right)^2 \xi_e = \dot{e} + \alpha e + \alpha \int_0^t e d\tau$$

Both SMC and PISMC gains used in the simulation are shown in Table 1. Note that the two sets of gains are identical. In this paper, these gains were tuned based on the results of simulations. The evaluation of such controllers was carried out in our simulation example.

For the first simulation, Fig. 2(a) shows the nonlinear system tracking performance with no external disturbances and an initial condition of $[\tilde{x}_d(0), \dot{\tilde{x}}_d(0)] = [\sin(\pi t/2), 0]$ with known bound function $a(t) = |\sin t| + 1$ [which verifies the assumed bound on $a(t)$]. It is evident that the PISMC presented in this paper is more effective than the SMC for reaching the desired state $\tilde{x}_d$ of the nonlinear system in less time. The stability and accuracy are both maintained in the tracking responses simulation.

For the second simulation, Fig. 2(b) shows the nonlinear system response. The initial condition is $[\tilde{x}_d(0), \dot{\tilde{x}}_d(0)] = (5, 0)$ with known bound function $a(t) = |\sin t| + 1$ (which verifies the assumed bound on $a(t)$. The results also verify that the PISMC is capable of tracking the desired states and the errors converge steadily to the neighborhood of zero, and Fig. 2(b) shows that $\tilde{x}_d$ settles down to the steady state and the amplitudes of the errors from the PISMC are smaller.

The conventional SMC and PISMC methods are simulated under the same conditions. By using a proportional-integral sliding surface, the performance of a control system can be adjusted with λ and α complementary parameters. The performance of the PISMC is better than that of the SMC.

Variations of the sliding signal for SMC and PISMC are illustrated in Fig. 2(c). Comparing the PISMC results with the SMC results shows that the PISMC has smaller chattering phenomenon. Variations of the sliding surface $s_{PI}(t)$ during the control are illustrated in Fig. 2(b) as well. The sliding surface is $s_{PI}(t) \neq 0$ when the error signal is not zero. When it reaches to the sliding surface, theoretically it is expected that the sliding function be zero (i.e. $s_{PI}(t) = 0$). In practical applications, there are always some small deviations and fluctuations at the output measured variable because of uncertainties and disturbances. Here, the average value of the sliding surface is zero $[s_{PI}(t) = 0]$. Thus, the control effort has smoothing, as shown in Figs. 2(a)–2(c). The effectiveness of this PISMC will be further validated by a simulated example and an experimental unmanned helicopter system in the following section.

Table 1. Selection of Controller Gains in Simulation

Controller designation	α	λ	η	Φ
SMC	—	0.6	20	0.1
PISMC	10	0.6	20	0.1

Unmanned Helicopter System Architecture

In 2006, the Remotely Piloted Vehicle and Microsatellite Laboratory (RMRL) of National Cheng Kung University (NCKU) started the H-LING program, which aimed to develop an unmanned helicopter system as a test-bed for control law research (Hsiao et al. 2007, 2008, 2009). Several versions of the H-LING unmanned helicopter system have been designed and modified. Although there are differences between each version, the main parts are almost the same; these consist of the vehicles, the attitude and positioning sensors, the onboard computer (OBC), and the ground control station (GCS). The present vehicles of H-LING are of the Thunder Tiger's Raptor-90 (R-90) model shown in Fig. 3(a). The R-90 has been the working vehicle since the beginning of the project. All the early system verifications and flight tests were conducted with the R-90. The R-90 is used as the controller testing platform because of its high mechanical design precision. The R-90 is still suitable for controller testing, and it has been flown numerous times to test the control laws. These flight tests will be described and discussed later.

In addition to the vehicles, an onboard hardware system is also essential. The central part of the onboard system is a PC/104-based single board computer. It is used because of its robustness and endurance under the harsh conditions of flight tests. The global positioning system (GPS) receiver and the attitude and heading reference system (AHRS) unit are also essential onboard sensors for offering basic state measurements. The wireless module is another necessary unit that connects the onboard system and the GCS. The vehicle alone is not sufficient to be a complete unmanned aerial vehicle (UAV). For most applications, the GCS is helpful in monitoring the vehicle's states or uploading commands to the vehicle to alter some settings or missions.

Onboard System

The H-LING adopts a PC/104-based single board computer as the main part of the OBC. A PCM-3380 with a PCM-3910 power board is used in the present onboard system. The PCM-3380 supports a compact flash (CF) card, and this allows the H-LING designer to install an operating system (OS) or to save data easily. Most users are more familiar with the Windows OS, which is another reason for H-LING to adopt it at this stage. An Xsens' MTi AHRS is used to offer attitudes and angular rates for the onboard controller. The outputs of MTi AHRS are Euler angles, angular rates, and accelerations. The MTi AHRS performs well in normal conditions; however, its outputs during the flight always contain unpredictable errors attributable to the engine's vibration. The

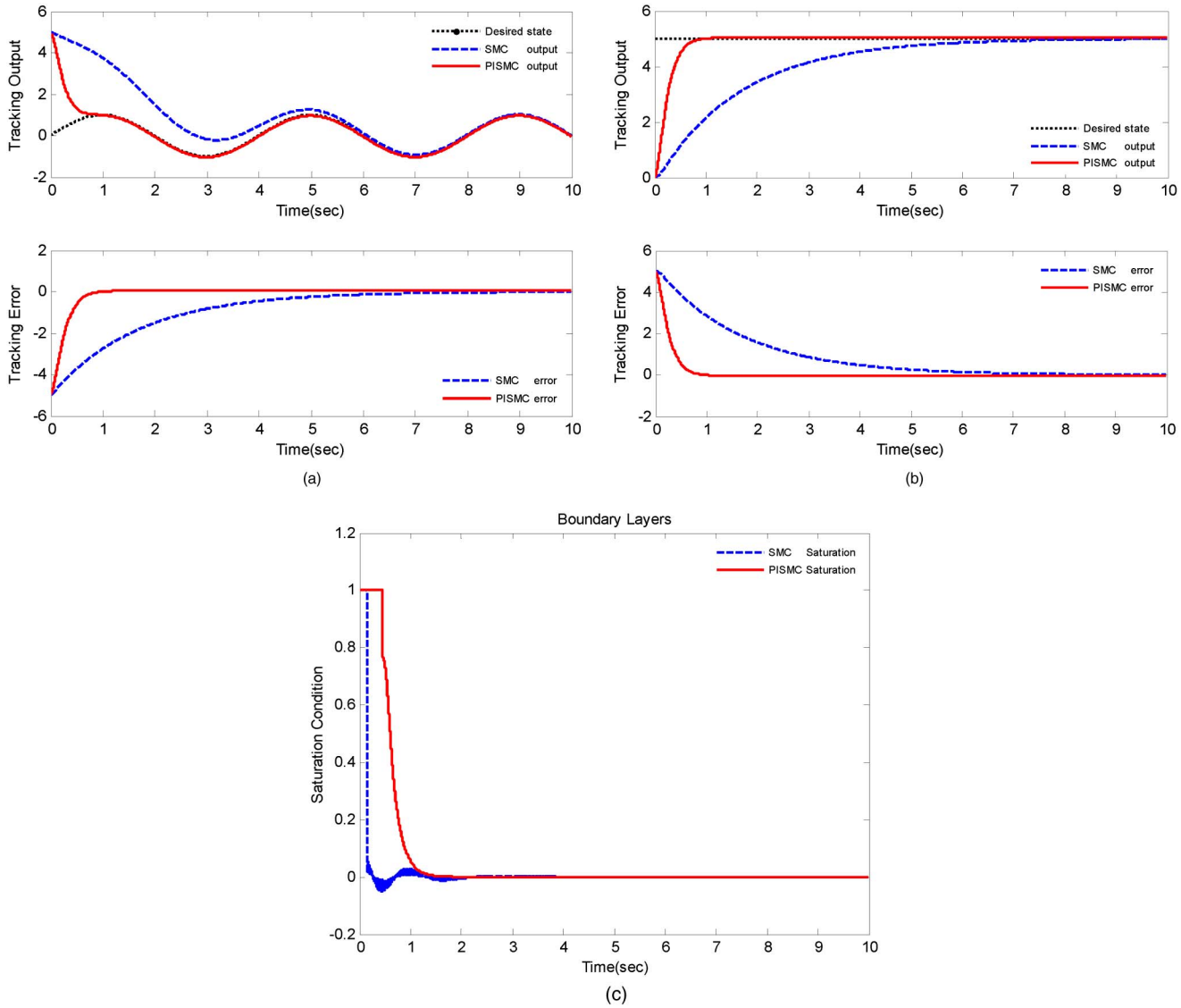

Fig. 2. (a) Comparison of system of tracking performance among various control methods; (b) comparison of response of systems among various control methods; (c) comparison of switching signals among various control methods

piston engine on the helicopter induces vibration and affects the onboard hardware to some extent. Therefore, vibration isolation or reduction becomes an important issue for the accuracy of the AHRS used in flight. Some vibration reduction materials were tested, and finally a kind of sound sheet for a car was chosen. The AHRS was surrounded by several layers of sound-deadening sheet and then cased into a box, as shown in Fig. 3(b).

In addition to the OBC, GPS, and AHRS, there is a homemade circuit board for control signal decoding/encoding and management. The H-LING integrated circuit board (HICB) is responsible for managing the control signals to the servos. There is a set of switches with relay on the HICB to handle these two control signals. The switch is set before flight, and then the pilot can use the RC transmitter to change the control modes between normal RC mode and autonomous mode during flight, as shown in Fig. 3(c).

Ground System

For a complete UAV, a GCS is necessary for monitoring and communicating with the airborne vehicle. The basic function of H-LING ground control station is receiving real-time data from the vehicle to monitor the status of the onboard system. In general operation, measurements from the AHRS and GPS are received by the GCS. Pulse-width modulation (PWM) control signals generated by the controller of OBC and the RC transmitter of the pilot are also monitored during flight tests. Furthermore, the GCS is able to upload certain commands to alter the control parameters or the testing modes. With the help of GCS, ground operators and the pilot can be aware of the vehicle's situation and then increase the safety and capability of the overall system. The core of the H-LING ground control station is the laptop with the corresponding program installed. Functions of the GCS program always follow the requirements of the overall system. For the former Windows OS, the GCS communicated with the onboard system via wireless module. The present GCS, however, can utilize the wireless local area networks (WLAN) as well as the wireless module (WM). Because the present onboard OS is the Windows embedded version, it is convenient for the GCS operator to access the onboard system via the WLAN through Bluetooth. This approach offers an alternative choice for the communication between the GCS and the onboard system when the distance between them is within about 2–3 m. The

(a)

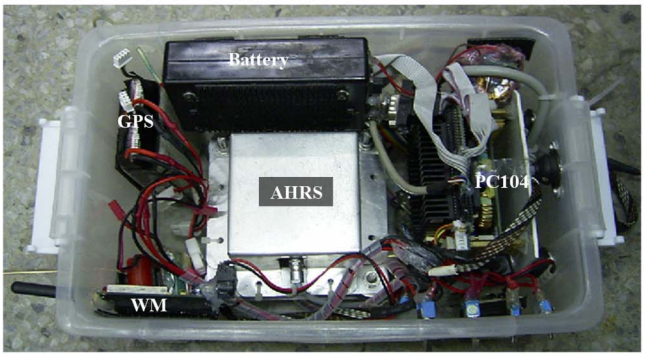

(b)

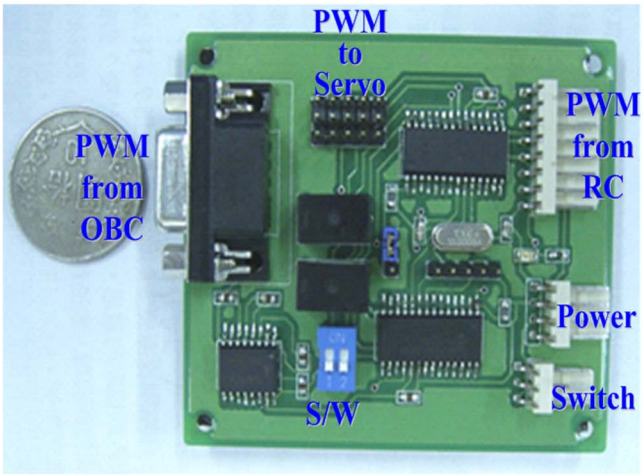

(c)

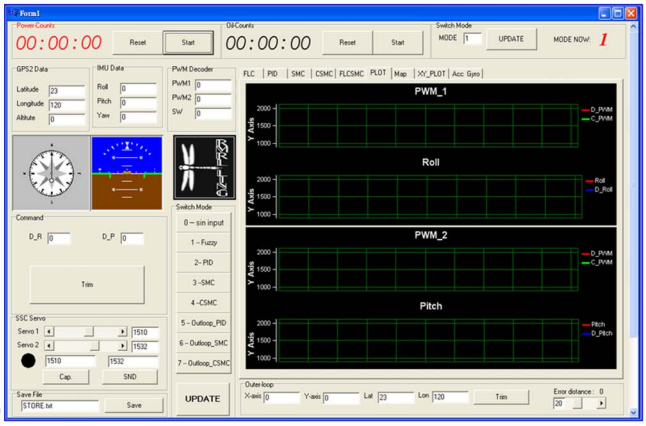

(d)

Fig. 3. (a) Vehicle of the H-LING unmanned helicopter system; (b) onboard avionics system; (c) H-LING integrated circuit board; (d) H-LING GCS interface for autonomous flight mission

GCS program provides communication interfaces between the ground test operators and the onboard system, as shown in Fig. 3(d). The panel with the black background in the bottom left corner can show the pilot's control signal history in real time. These real-time outputs on the GCS screen give valuable references for control gain tuning and control law improvement. The ground operators obtain this information immediately and can make corresponding decisions promptly. Thus, the flight experiments are more efficient. The overall system installed on the vehicle is shown in Fig. 4.

Unmanned Helicopter Model

Consider a body-fixed frame attached on a rotorcraft (Mettler 2003), as shown in Fig. 5. The force and moment equations of the helicopter in the body frame are shown as follows:

$$\dot{u} = (-wq + vr) + X/m \qquad \dot{v} = (-ur + wp) + Y/m$$
$$\dot{w} = (-vp + up) + Z/m \qquad \dot{p} = -qr(I_{yy} - I_{ZZ})/I_{xx} + L/I_{xx}$$
$$\dot{q} = -pr(I_{zz} - I_{xx})/I_{yy} + M/I_{yy}$$
$$\dot{r} = -pq(I_{xx} - I_{yy})/I_{zz} + N/I_{zz} \tag{17}$$

Note that X, Y, and Z = forces along three body axes x, y, z, respectively; L, M, and N = moments; I_{xx}, I_{yy}, and I_{zz} = moments of inertia; u, v, and w = velocities; $\dot{u}$ and $\dot{v}$ = fuselage lateral and longitudinal motion, respectively; $\dot{w}$ = fuselage vertical motion; p, q, and r = angular rates; $\dot{p}$ and $\dot{q}$ = roll and pitch motion, respectively; $\dot{r}$ = fuselage yaw motion; and m = mass of helicopter.

Taking the hovering condition as the equilibrium point, the motion equations can be linearized. Furthermore, by introducing the coupling effect in the main rotor, we can obtain the following equations as described in Mettler (2003) and Hsiao et al. (2007)

$$\dot{u} = -g\theta + X_u u + X_a a \qquad \dot{v} = g\phi + Y_v v + Y_b b + Y_{\text{ped}}\delta_{\text{ped}}$$
$$\dot{w} = -Z_a a + Z_b b + Z_w w + Z_r r + Z_{\text{col}}\delta_{\text{col}}$$
$$\dot{p} = L_u u + L_v v + L_b b + L_w w$$
$$\dot{q} = M_u u + M_v v + M_a a + M_w w + M_{\text{col}}\delta_{\text{col}}$$
$$\dot{r} = N_v v + N_p p + N_w w + N_r r + N_r r + N_{\text{ped}}\delta_{\text{ped}} + N_{\text{col}}\delta_{\text{col}} \tag{18}$$

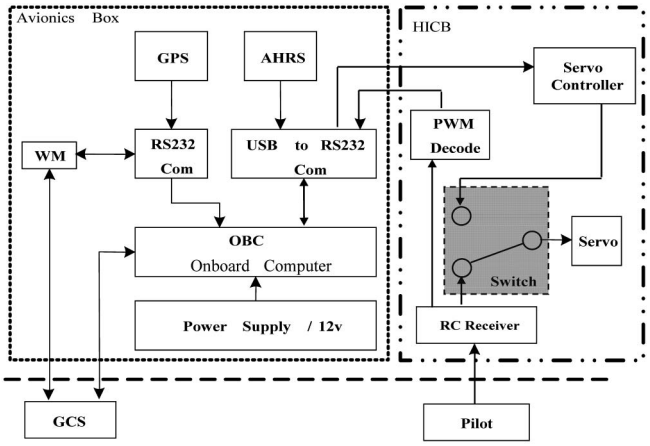

Fig. 4. Onboard avionics system architecture of unmanned helicopter system

where δ_{ped} and δ_{col} = pedal input and the collective input, respectively; θ and ϕ = Euler angles; a and b are longitudinal and lateral rotor flapping angles, respectively; and the acceleration attributable to gravity is denoted by g. The subscripts in the previous equations denote the partial derivatives with respect to the subscripted parameters.

For the remote-controlled helicopter used in this study, an off-the-shelf controller automatically stabilized the helicopter's heading using feedback on a gyroscope signal. Therefore, fuselage yaw motion equation $\dot{r}$ can be presented with the following equations:

$$\dot{r} = N_v v + N_r r + N_{\text{ped}}(\delta_{\text{ped}} - r_{fb}) \tag{19}$$

$$\dot{r}_{fb} = -K_{\text{rfb}} r_{fb} + K_r r \tag{20}$$

where r_{fb} = feedback control signal from the gyroscope.

In addition to yaw rate gyro, another important characteristic of a small-scale rotorcraft is the installation of the flybar, sometimes called the stabilizer bar. The flybar was first used in the 1950s with a Bell-Hiller-mixer to increase the performance and stability of a helicopter. The stabilizer bar is usually regarded as a secondary rotor, meaning that it only stabilizes the system but does not provide thrust. Hence, no collective pitch is used on it. The flybar dynamics are also viewed as feedback to the main rotor dynamics (Mettler 2003).

Accordingly, the rolling and the pitching equations of motion of the stabilizer bar are

$$\tau_f \dot{a} = -a - \tau_f q + A_b b + A_{\text{lon}} \delta_{\text{lon}} \tag{21}$$

$$\tau_f \dot{b} = -b - \tau_f p + B_a a + B_{\text{lat}} \delta_{\text{lat}} \tag{22}$$

where δ_{lat} and δ_{lon} = cyclic lateral input and cyclic longitudinal input, respectively; τ_f = main rotor time constant; τ_s = stabilizer bar time constant; and A_{lon} = longitudinal stick to cyclic pitch gearings; and B_{lat} = lateral stick to cyclic pitch gearings. The subscripts in the above equations denote the partial derivative with respect to the subscripted parameters. The heading equations of motion of the stabilizer bar are

$$\tau_s \dot{c} = -c - \tau_s q + C_{\text{lon}} \delta_{\text{lon}} \tag{23}$$

$$\tau_s \dot{d} = -d - \tau_s q + D_{\text{lon}} \delta_{\text{lon}} \tag{24}$$

The complete model of the linearized dynamics model is as follows:

$$\begin{bmatrix} \dot{u} \\ \dot{v} \\ \dot{p} \\ \dot{q} \\ \dot{\phi} \\ \dot{\theta} \\ \tau_f \dot{a} \\ \tau_f \dot{b} \\ \dot{w} \\ \dot{r} \\ \dot{r}_{fb} \\ \tau_s \dot{c} \\ \tau_s \dot{d} \end{bmatrix} = \begin{bmatrix} X_u & 0 & 0 & 0 & 0 & -g & X_a & 0 & 0 & 0 & 0 & 0 & 0 \\ 0 & Y_v & 0 & 0 & g & 0 & 0 & Y_b & 0 & 0 & 0 & 0 & 0 \\ L_u & L_v & 0 & 0 & 0 & 0 & 0 & L_b & L_w & 0 & 0 & 0 & 0 \\ M_u & M_v & 0 & 0 & 0 & 0 & M_a & 0 & M_w & 0 & 0 & 0 & 0 \\ 0 & 0 & 1 & 0 & 0 & 0 & 0 & 0 & 0 & 0 & 0 & 0 & 0 \\ 0 & 0 & 0 & 1 & 0 & 0 & 0 & 0 & 0 & 0 & 0 & 0 & 0 \\ 0 & 0 & 0 & -\tau_f & 0 & 0 & -1 & A_b & 0 & 0 & 0 & A_c & 0 \\ 0 & 0 & -\tau_f & 0 & 0 & 0 & B_a & -1 & 0 & 0 & 0 & 0 & B_d \\ 0 & 0 & 0 & 0 & 0 & 0 & Z_a & Z_b & Z_w & Z_r & 0 & 0 & 0 \\ 0 & N_v & N_p & 0 & 0 & 0 & 0 & 0 & N_w & N_r & N_{\text{rfb}} & 0 & 0 \\ 0 & 0 & 0 & 0 & 0 & 0 & 0 & 0 & 0 & K_r & K_{\text{rfb}} & 0 & 0 \\ 0 & 0 & 0 & -\tau_s & 0 & 0 & 0 & 0 & 0 & 0 & 0 & -1 & 0 \\ 0 & 0 & -\tau_s & 0 & 0 & 0 & 0 & 0 & 0 & 0 & 0 & 0 & -1 \end{bmatrix} \begin{bmatrix} u \\ v \\ p \\ q \\ \phi \\ \theta \\ \tau_f a \\ \tau_f b \\ w \\ r \\ r_{fb} \\ \tau_s c \\ \tau_s d \end{bmatrix} + \begin{bmatrix} 0 & 0 & 0 & 0 \\ 0 & 0 & Y_{\text{ped}} & 0 \\ 0 & 0 & 0 & 0 \\ 0 & 0 & 0 & M_{\text{col}} \\ 0 & 0 & 0 & 0 \\ 0 & 0 & 0 & 0 \\ A_{\text{lat}} & A_{\text{lon}} & 0 & 0 \\ B_{\text{lat}} & B_{\text{lon}} & 0 & 0 \\ 0 & 0 & 0 & Z_{\text{col}} \\ 0 & 0 & N_{\text{ped}} & N_{\text{col}} \\ 0 & 0 & 0 & 0 \\ 0 & C_{\text{lon}} & 0 & 0 \\ D_{\text{lat}} & 0 & 0 & 0 \end{bmatrix} \begin{bmatrix} \delta_{\text{lat}} \\ \delta_{\text{lon}} \\ \delta_{\text{ped}} \\ \delta_{\text{col}} \end{bmatrix} \tag{25}$$

Attitude Control Design

The unmanned helicopter can be described by the linear multi-input-multioutput (MIMO) system, and the equation of motion of the entire system could be rearranged and presented in the state space form

$$\dot{\hat{x}} \hat{x} \hat{F} \hat{x} + \hat{G} \hat{u} + \hat{D}(\hat{x}, t) \tag{26}$$

The system state vector is defined by

$$\hat{x} = \begin{bmatrix} \hat{x}_1 & \hat{x}_2 & \dots & \hat{x}_n \end{bmatrix}^T = \begin{bmatrix} u & v & w & p & q & \phi & \theta & a & b & r & r_{fb} & c & d \end{bmatrix}^T$$

The PISMC input vector $\hat{u}$ is

$$\hat{u} = \begin{bmatrix} \hat{u}_1 & \hat{u}_2 & \dots & \hat{u}_m \end{bmatrix}^T = \begin{bmatrix} \delta_{\text{lat}} & \delta_{\text{lon}} & \delta_{\text{ped}} & \delta_{\text{col}} \end{bmatrix}^T$$

Assume that there is a system state vector

$$\hat{x} = \begin{bmatrix} \hat{x}_1 & \hat{x}_2 & \dots & \hat{x}_n \end{bmatrix}^T$$

and $\hat{u}$ is the control input ($m < n$); $\hat{F} \in R^{n \times n}$ and $\hat{G} \in R^{n \times n}$ are known constant matrices. The control problem is to get the state $\hat{x}$ to track a desired state $\hat{x} = \begin{bmatrix} \hat{x}_{d1} & \hat{x}_{d2} & \dots & \hat{x}_{dn} \end{bmatrix}^T$ in the presence of model uncertainty on $\hat{F}$ and $\hat{G}$. The external disturbance $\hat{D}$ is defined as

$$\| \hat{D}(\hat{x}, t) \| \le \hat{\sigma}(\hat{x}, t) \tag{27}$$

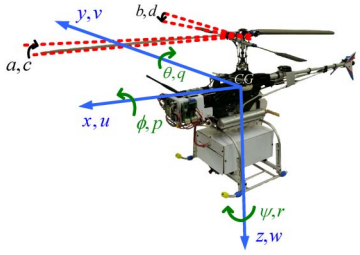

Fig. 5. Definition of body-fixed frame

where $\hat{\sigma}(\hat{x},t)$ is a known upper-bounded function. Let $\hat{e}_1 = \hat{x}_1 - \hat{x}_{d1}$ be the tracking error in the variable $\hat{x}_1$, and let

$$\hat{e} - \begin{bmatrix} \hat{e}_1 & \hat{e}_2 & \dots & \hat{e}_n \end{bmatrix}^T \tag{28}$$

be the tracking error vector. The PISMC sliding surface is modified from the aforementioned s_{PI}, and it has form

$$\hat{S}_{PI} = \hat{S}_P + \hat{S}_I = \hat{C}\hat{E} \tag{29}$$

where

$$\hat{E} = \hat{e} + \hat{\xi}, \qquad \hat{\xi}_e = \begin{bmatrix} \int_0^t \hat{e}_1 d\tau & \int_0^t \hat{e}_2 d\tau & \dots & \int_0^t \hat{e}_n d_\tau \end{bmatrix}^T,$$
$$\hat{S}_{PI} = \begin{bmatrix} \hat{S}_{PI_1} & \hat{S}_{PI_2} & \dots & \hat{S}_{PI_m} \end{bmatrix}^T, \qquad \hat{C} \in R^{m\times n}$$

are known constant matrices. The existence of the $\hat{C}\hat{G}$ inverse is a necessary condition. Once the sliding surface has been determined, we may start to design the controller and the sliding condition of the PISMC as follows

$$\hat{S}_{PI}^T \dot{\hat{S}} \hat{S}_{PI} < -\eta \|\hat{S}_{PI}\|, \qquad \hat{S}_{PI} \neq 0 \qquad \eta > 0 \tag{30}$$

The PISMC approach is to find $\hat{u}$ such that the state trajectory stays on the sliding surface $\hat{S}_{PI} = 0$. The PISMC is found by recognizing that $\dot{\hat{S}}_{PI} = 0$ is a necessary condition for the state trajectory to stay on the sliding surface $\hat{S}_{PI} = 0$. Differentiating $\hat{S}_{PI}$ with respect to time along the trajectory of Eqs. (26) and (28) gives

$$\dot{\hat{S}}_{PI} = \hat{C}\dot{\hat{E}} = \hat{C}(\dot{\hat{e}} + \dot{\hat{\xi}}_e) = \hat{C}(\dot{\hat{x}} - \dot{\hat{x}}_d + \hat{x} - \hat{x}_d) = 0 \tag{31}$$

Substituting Eq. (26) into Eq. (31) and rearranging to solve for $\hat{u}$ yields

$$\hat{u} = -(\hat{C}\hat{G})^{-1}\hat{C}\hat{F}\hat{x} - (\hat{C}\hat{G})^{-1}\hat{C}(\dot{\hat{x}}\hat{x}_d - \dot{\hat{x}}_d)$$
$$- (\hat{C}\hat{G})^{-1}(\gamma + \eta)\text{sat}(\hat{S}_{PI}, \Phi) \tag{32}$$

where $\gamma = \|\hat{C}\|\hat{\sigma}(\hat{x},t)$. The function $\text{sat}(\hat{S}_{PI}, \Phi)$ is the saturation function defined by

$$\text{sat}(\hat{S}_{PI}, \Phi) = \begin{cases} (\hat{S}_{PI})/(\|\hat{S}_{PI}\|) & \text{if } \|\hat{S}_{PI}\| > \Phi \\ (\hat{S}_{PI})/\Phi & \text{if } \|\hat{S}_{PI}\| \leq \Phi \end{cases} \tag{33}$$

According to the PISMC $\hat{u}$, the state trajectories are driven and attracted toward the sliding surface and satisfy the sliding conditions as in Eq. (30). The architecture of PISMC is shown in Fig. 6.

Simulation Results for Attitude Controller Design

In this section, a numerical simulation of PISMC as applied to an unmanned helicopter system is presented. The dynamics of the unmanned helicopter system are defined in Eq. (26), and in the simulation, the parameters of the system model used are shown in Table. 2 (Mettler 2003; Hsiao et al. 2007). The system external disturbance D is assumed, and the PISMC gain parameters used are shown in Table. 3.

Fig. 7 shows the system responses of the helicopter's attitude with external disturbances. To examine the disturbance rejection property of the proposed control, we consider the disturbance $D = \sin(3\pi t)$ and simulate the system with initial condition $[\hat{x}_d(0), \dot{\hat{x}}\hat{x}_d(0)] = (5,0)$. We note that the settling time to reach $\hat{x}_d$ and the error of the PISMC are not only smaller but also converge more quickly than the values given by the conventional SMC. Comparing the PISMC results with the SMC results shows that the PISMC has smaller overshoot, smaller rise time, and smaller settling time than the conventional SMC. It is proven that the PISMC presented in this paper is effective for the helicopter's attitude to reach the desired attitudes in short periods around the equilibrium point. The stability and accuracy are both maintained in the hovering simulation.

The results also show that the PISMC is capable of tracking the desired angle and that the errors converge steadily to the neighborhood of zero. Thus, the control effort has smoothing, and the PISMC has a smaller chattering phenomenon, as shown in Fig. 7.

Flight Test Results for Attitude Controller Verification

The results in the first part of the paper support the goal of developing an autonomous hovering capacity for the H-LING unmanned helicopter (Hsiao et al. 2007; Hsiao et al. 2008). All the efforts are concentrated on the hovering control design. Therefore, a series of flight tests were conducted for the controller verification. The design of the HICB allows the onboard system to record PWM control signals from both the OBC and the pilot at the same time.

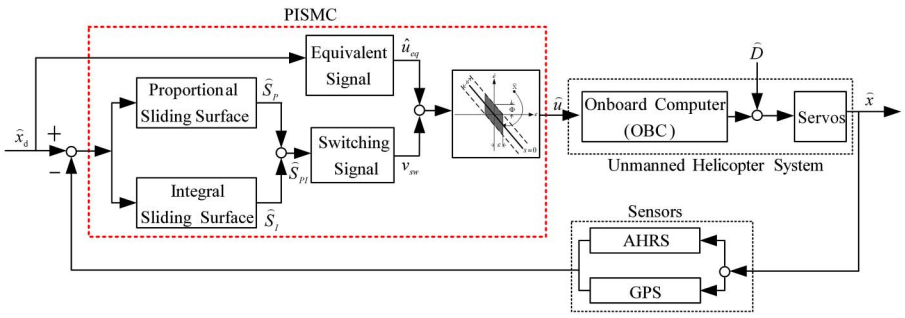

Fig. 6. Architecture of PISMC

Table 2. Parameters of Unmanned Helicopter Obtained from System Identification

Matrix parameter									
Parameter (unit)	Value	Parameter (unit)	Value	Parameter (unit)	Value	Parameter (unit)	Value	Parameter (unit)	Value
X_u $(1/s^2)$	$-g$	M_u $(1/s^2)$	−0.051	τ_f (s)	0.054	N_w (1/s)	0.08	Y_{ped} (1/s)	—
X_a $(1/s^2)$	$-g$	M_v $(1/s^2)$	−0.05	τ_s (s)	0.227	N_r (1/s)	−4.7	M_{col} $(1/s^2)$	
Y_v (rad $*$ m/s^2)	−0.4	M_a $(1/s^2)$	215.6	Z_w $(1/s^2)$	−16.2	N_{rfb} (1/s)	−2,843.76	A_{lat}	0.0313
Y_b (rad $*$ m/s^2)	G	M_w $(1/s^2)$	—	Z_r $(1/s^2)$	0.93	K_r	0.376	A_{lon}	−0.1
L_u $(1/s^2)$	−0.1	A_b	−0.189	Z_a $(1/s^2)$	−9.75	K_{rfb}	9.7	B_{lat}	0.14
L_v $(1/s^2)$	0.3	A_c	0.76	Z_b $(1/s^2)$	−131	N_{col} $(1/s^2)$	−3.4	B_{lon}	0.01
L_b $(1/s^2)$	326	B_a	0.368	N_v (1/s)	0.0301	Z_{col} (1/s)	85.5	C_{lon}	−0.29
L_w $(1/s^2)$	—	B_d	0.76	N_p (1/s)	−3.53	N_{ped} $(1/s^2)$	2,843.76	D_{lat}	0.3

Table 3. Selection of Controller Gains of Unmanned Helicopter

Controller designation		α	λ	η	Φ
SMC	Roll	—	5	15	1
	Pitch		3	20	3
PISMC	Roll	7.05	5	15	1
	Pitch	0.9	3	20	3

The simultaneously recorded data are helpful in examining the performance of the controller. Comparing the PWM signals from the OBC and the pilot, the designer could determine whether the controller performances are reasonable, as shown in Fig. 8. In Fig. 8, the autopilot was not engaged. The solid line presents the rolling and pitching control signal from the pilot, and the dashed line is the one from the PISMC in the OBC program. The inputs of roll and pitch that are controlled by the PISMC followed the recorded actual control signal from the ground pilot. This demonstrates that the PISMC could give reasonable control inputs in the roll and pitch motions during the real flight.

Fig. 9(a) and 9(b) shows the results of the second goal of this paper. We successfully designed PISMC for the H-LING unmanned helicopter system by using the techniques in previous sections. A series of successful flight tests was conducted at an open area along the seaside near An-Ping Port, located in the southern part of Taiwan. Typically, the unmanned helicopter would take off manually under pilot control and reach a nominal altitude ranging from 10 m to 15 m. Then, when the unmanned helicopter was brought into a steady-state hovering condition, the autonomous hovering would be engaged by the pilot. Fig. 9(a) and 9(b) show

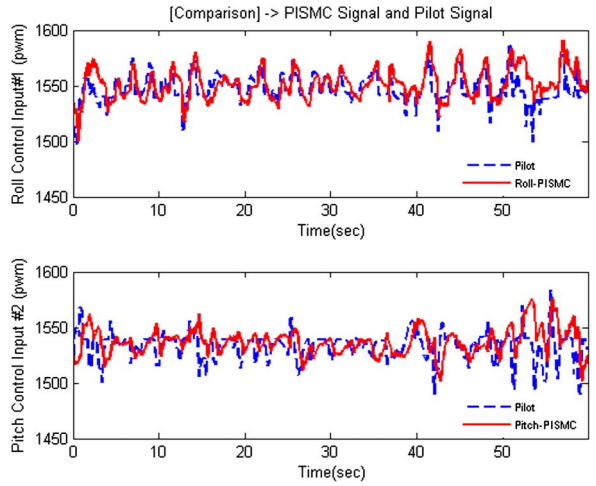

Fig. 8. Comparison of command signal of PISMC and that of pilot signal

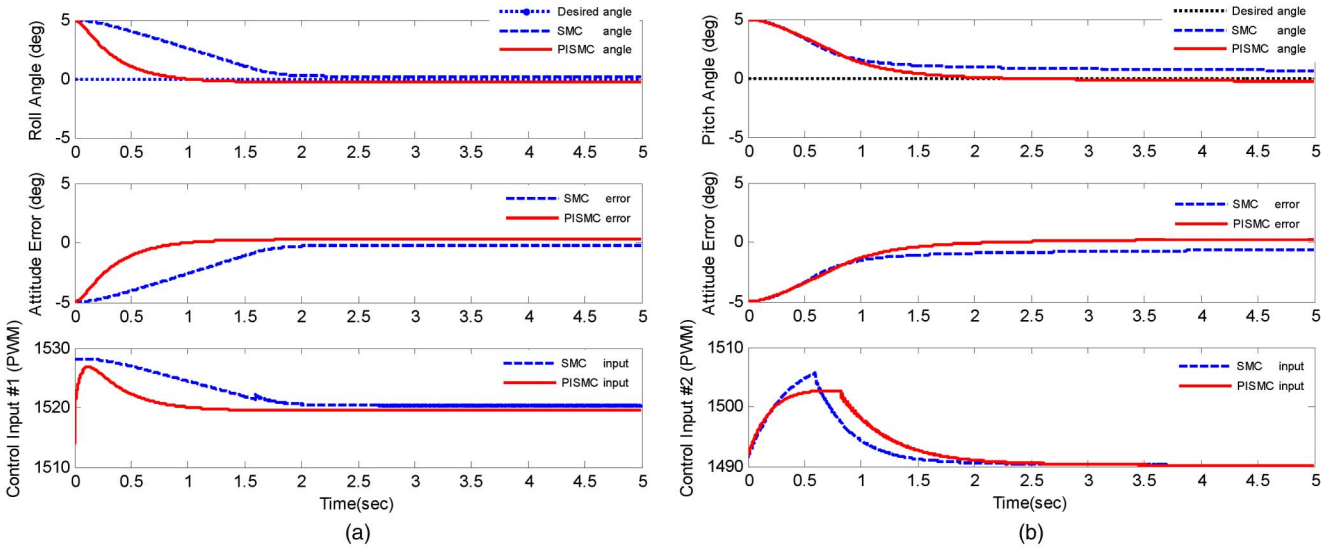

Fig. 7. (a) Comparison of rolling response of system among various methods with disturbances; (b) comparison of pitching response of system among various methods with disturbances

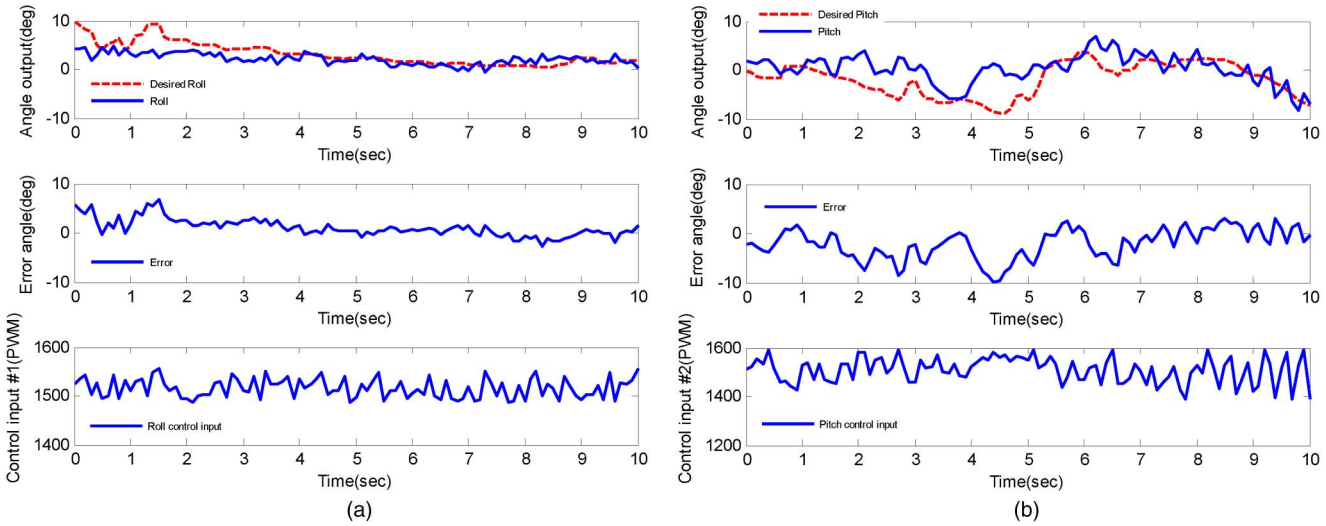

Fig. 9. (a) Result of roll control; (b) result of pitch control

the results of flight test under external disturbances (crosswind). Both the roll and pitch errors were kept within 5° throughout the automatic flight phase.

More importantly, the flight tests result shows that the PISMC holds the autonomous hovering well for the developed unmanned helicopter system. Other motions, however, are not included in the autonomous hovering test. The heading control of the helicopter was left for the gyro, which is equipped on almost all conventional RC helicopters. The gyro held the vehicle's heading with extremely good stability and therefore reduced the difficulty of the preliminary autonomous hovering control.

Conclusions

The research presented in this paper focuses on the design of a hovering control system for an unmanned helicopter system. Based on the advantages and disadvantages of the conventional SMC, this paper derived a PISMC that retains the advantages of the SMC while mitigating its drawbacks. In this work, the complete linearized dynamics model was used in simulations to validate the PISMC design, and simulation results showed that the PISMC outperformed the SMC. In the tracking simulations, the tracking errors of the PISMC were smaller and converge more rapidly than those of the conventional SMC.

To realize a hovering control for an unmanned helicopter system using the PISMC, this paper developed an unmanned helicopter system as the experimental platform. Some of the major outcomes of this paper as follows:

- Development of hardware and software of an onboard avionics system capable of performing data acquisition task and managing automatic flights;
- Development of an interactive ground control station software that enables real-time, continuous data-link communication between the airborne UAV and ground operating personnel;
- Validation of the PISMC controllers in both computer simulations and actual flight tests; and
- Development of reliable and more compact onboard architecture with HICB.

The PISMC and the conventional SMC were investigated in the presented study. The design of PISMC is able to achieve the desired control requirement more precisely and also stabilize the system's inner loop. The PISMC has advantages over the conventional SMC in several aspects. For example, two complementary parameters are available for the PISMC to tune for better system response performance. Furthermore, the PISMC has improved the chattering phenomenon that is common and unavoidable in the conventional SMC, as shown in Figs. 2 and 7. Successful computer simulations and flight test results validate that the proposed method is practical and the PISMC is verified to be capable of being employed on an unmanned helicopter system for attitude control.

Acknowledgments

This research is supported by National Science Council of Taiwan under research grant NSC-98-2623-E-006-013-D, which is greatly appreciated.

References

Baik, I. C., Kim, K. H., and Youn, M. J. (2000). "Robust nonlinear speed control of PM synchronous motor using boundary layer integral sliding mode control technique." *IEEE Trans. Control Syst. Technol.*, 8(1), 47–54.

Bouabdallah, S., and Siegwart, R. (2005). "Backstepping and sliding mode techniques applied to an indoor micro quad-rotor." *Int. Conf. on Robotics and Automation*, IEEE, 2259–2264.

Chen, C. A., Chiang, H. K., and Lin, B. R. (2008). "The novel adaptive sliding mode position control synchronous reluctance motor drive." *Journal of the Chinese Society of Mechanical Engineers*, 29(3), 241–247.

Chen, Y. P., and Her, W. C. (1992). "Bang-bang controller design for servomechanisms using the sliding-mode theory." *Proc. Int. Conf. on Intelligent Control and Instrumentation*, IEEE, 312–316.

Chern, T. L., and Wu, Y. C. (1991). "Design of integral variable structure controller and application to electrohydraulic position servo control system." *IEE Proc-D, Control Theory and Applications*, 138(5), 439–444.

Edwards, C., and Spurgeon, S. K. (1998). *Sliding mode control: Theory and applications*, Taylor and Francis, London.

Fung, R. F., Wang, Y. C., and Huang, H. H. (1997). "A variable structure control with proportional and integral compensations for electrohydraulic system." *Mechatronics*, 7(1), 67–81.

Hess, R. A., and Wells, S. R. (2002). "Sliding mode control applied to reconfigurable flight control design." *40th AIAA Aerospace Sciences Meeting and Exhibit*, Reno, NV, 1–12.

Hsiao, F. B., et al. (2007). "An unmanned helicopter vehicle system development." *12th Australian Int. Aerospace Congress*, Melbourne, Australia, 20–27.

Hsiao, F. B., et al. (2009). "The development of advanced technology, system integration and their verifications and applications for military's unmanned aerial vehicle system." *National Defense Science and Technology Academic Conf.*, Taoyuan, Taiwan, ROC, 28–35.

Hsiao, F. B., Lin, C. H., Ding, Y. R., and Liu, N. Y. (2008). "Unmanned aerial helicopter autonomous flight research: Attitude stabilization robustness of hovering flight." *National Defense Science and Technology Academic Conf.*, Taoyuan, Taiwan, ROC, 30–37.

Hu, Q., Cao, J., and Zhang, Y. (2009). "Robust backstepping sliding mode attitude tracking and vibration damping of flexible spacecraft." *J. Aerosp. Eng.*, 22(2), 139–152.

Mettler, B. (2003). *Identification modeling and characteristics of miniature rotorcraft*, Kluwer Academic, Boston.

Niu, Y., Ho, D. W. C., and Lam, J. (2005). "Robust integral sliding mode control for uncertain stochastic systems." *Automatica*, 41, 873–880.

Sira-Ramirez, H., Zribi, M., and Ahmad, S. (1994). "Dynamical sliding mode control approach for vertical flight regulation in helicopters." *IEE Proc-D, Control Theory and Applications*, 141(1), 19–24.

Slotine, J. J. E. (1984). "Sliding controller design for nonlinear systems." *International Journal of Control*, 40(2), 421–434.

Slotine, J. J. E., and Li, W. (1991). *Applied nonlinear control*, Prentice-Hall, Upper Saddle River, NJ.

Su, J. P., and Wang, C. C. (2002). "Complementary sliding control of non-linear systems." *International Journal of Control*, 75(5), 360–368.

Utkin, V. I. (1977). "Variable structure with sliding mode-A Survey." *IEEE Trans. Autom. Control*, 22(2), 212–222.

Utkin, V. I., and Shi, J. (1996). "Integral sliding mode in systems operating under uncertainty conditions." *Proc. of the 35th Conf. on Decision and Control*, IEEE, 4591–4596.

Waslander, S. L., Hoffmann, G. M., Jang, J. S., and Tomlin, C. J. (2005). "Multi-agent quad-rotor test-bed control design: integral sliding mode vs. reinforcement learning." *IEEE/RSJ Int. Conf. on Intelligent Robots and Systems*, 468–473.

Yang, C. D., and Kung, C. C. (2000). "Nonlinear H_∞ flight control of general six-degree-of-freedom motions." *J. Guid. Control. Dyn.*, 23(2), 278–288.